ATOMIC WIRES

Ultralong sheathed single-metal-atom chains synthesized under high pressure

Jie Zhang[1], Xiao Dong[2], Shengchao Qiu[2], Xin Yang[1], Chengyu Li[1], Hongfei Ma[3], Yunfan Fei[1], Qingchao Zeng[1], Fang Li[1], Yi Xie[4], Yan Duan[4], Xudong Jiang[1], Jingqin Xu[1], Puyi Lang[1], Jiarui Yuan[1], Hao Luo[1], Yuan Fang[1], Zilin Zhao[1], Yikun Bao[1], Yajie Wang[1], Yongjin Chen[1], Junliang Sun[3], Shangda Jiang[4,5], Ho-kwang Mao[1], Haiyan Zheng[1], Kuo Li[1]*

Single-metal-atom chains (SMACs) represent the ultimate limit of one-dimensional nanostructures. They serve as archetypal model systems for condensed matter physics and constitute fundamental building blocks for next-generation nanoelectronics. However, synthesis of SMACs suitable for practical applications remains challenging. In this work, we create micrometer-long, carbon-sheathed copper SMACs at milligram scale by compressing β-copper phthalocyanine to above 21 gigapascals. The SMACs are in atom-scale ordering, are isolable through acid-assisted exfoliation, and exhibit exceptional stability, with Cu-Cu distance confined at 2.57 angstroms. Anisotropic conductance and antiferromagnetic interactions are suggested by experimental and computational results. This work establishes a universal synthetic strategy for sheathed SMACs, positioning them as a compelling platform for prospective electronic and spintronic applications.

Single-metal-atom chains (SMACs) are regarded as the thinnest metal wires. As a representative one-dimensional (1D) structure at the ultimate scaling limit, SMACs attract substantial interest across fields, including electronics (*1*, *2*), magnetism (*3*–*5*), optics (*6*, *7*), and catalysis (*8*), and serve as an ideal model for investigating various condensed matter theories, such as Peierls instabilities (*9*, *10*) and the Tomonaga-Luttinger liquid (*11*). Particularly in the current post-Moore era—where silicon-based chips are approaching their fundamental physical size limits—the potential application of SMACs as molecular wires is also emerging (*12*, *13*).

Over recent decades, several synthetic routes for SMACs have been developed (*14*). Typically, SMACs require a support for stabilization, including surfaces (*3*, *11*, *15*), grain boundaries (*16*, *17*), and organic ligands (*13*). Among them, organic ligand–assisted synthesis, typically conducted in solution, not only provides enhanced flexibility in structural control but also enables the scalable synthesis of various SMACs, such as Cr, Fe, Co, Ni, Cu, Pt, Ru, and Rh (*12*, *13*, *18*, *19*). However, most reported SMACs consist of fewer than 10 metal atoms. A primary reason is that the solution-phase synthesis usually requires a soluble ligand to assist the formation of SMACs, but ligands that can match the expected length of SMACs are often insoluble. Only several studies on Ni-SMACs have documented structures containing 11 atoms and above (*20*, *21*), with the current record being 28 atoms (*22*). The lack of a popular synthetic method has severely prohibited its further research and application.

[1]Center for High Pressure Science and Technology Advanced Research, Beijing, P.R. China. [2]Key Laboratory of Weak-Light Nonlinear Photonics, School of Physics, Nankai University, Tianjin, P.R. China. [3]College of Chemistry and Molecular Engineering, Peking University, Beijing, P.R. China. [4]Spin-X Institute, School of Chemistry and Chemical Engineering, State Key Laboratory of Luminescent Materials and Devices, Guangdong-Hong Kong-Macao Joint Laboratory of Optoelectronic and Magnetic Functional Materials, South China University of Technology, Guangzhou, P.R. China. [5]Quantum Science Center of Guangdong-Hong Kong-Macao Greater Bay Area, Shenzhen, P.R. China. ***Corresponding author. Email: likuo@hpstar.ac.cn**

High pressure provides a solid-state reaction route to avoid the solubility problem during synthesis. Numerous extended 1D materials with exceptional mechanical strength, such as diamond nanothreads (DNThs), have been synthesized from columnarly stacked planar molecules (*23*–*26*). From suitable annular molecular precursors, a nanotube can be obtained, which is ideal for encapsulating metastable 1D systems. Crucially, applied pressure can directly compress the metal-metal distances of the planar coordination compounds, together with the transformation from organic ligand to polymerized carbon frameworks, which will lock the compressed metal-metal distance through the coordination bonds (Fig. 1).

In this work, we applied external pressure exceeding 21 GPa on single-crystal β-copper phthalocyanine (CuPc) and obtained extended sheathed Cu-SMACs in single-crystal form. The Cu atoms are locked by the coordination N-Cu bonds with an interatomic Cu-Cu distance of 2.57 Å, and the Cu-SMACs are sheathed by sp^3-carbon networks, forming sheathed single-metal-atom chains (sSMACs). Synergistically, the dense atomic packing and the encapsulating sp^3-carbon network endow the Cu-SMACs with marked robustness against ambient air and even strongly acidic media, prominent 1D antiferromagnetic coupling, and anisotropic electrical conduction. This combination of properties positions sSMACs as a highly promising material platform for future nanoelectronic and spintronic devices.

Synthesis and in situ exploration of Cu-sSMACs

CuPc, also called phthalocyanine blue, is a famous synthetic blue pigment, which usually crystallizes in a monoclinic phase (β-phase, space group $P2_1/n$) at ambient conditions. The CuPc molecules are parallelly stacked in columns with a slip angle of 45.5° (Fig. 2A). Using physical vapor transport, we prepared purple rectangular single crystals of β-CuPc. The crystal elongates along the *b* axis, which is the direction of molecular stacking, and the magnitude of *b* directly corresponds to the Cu-Cu distance between adjacent CuPc molecules. We investigated the evolution of unit cell parameters of β-CuPc from ambient pressure to 21.5 GPa by using in situ high-pressure single-crystal x-ray diffraction (SCXRD) (fig. S1). β-CuPc transforms into a high-pressure phase (referred to as HP-CuPc) at 0.9 GPa, as indicated by the abrupt change of the unit cell parameters (fig. S2). The crystal structure of HP-CuPc was determined by geometry optimization after Rietveld refinement of high-pressure powder x-ray diffraction (fig. S3, A and B). It preserves the space group and the intercolumnar packing of β-CuPc but exhibits a substantially reduced *b* axis (3.44 Å versus 4.79 Å in β-CuPc) and a slip angle changed from 45.5° to 28.6° at 4.3 GPa (Fig. 2B). The intracolumnar packing of HP-CuPc is similar to that of the reported η-CuPc (*27*, *28*), but it exhibits a different intercolumnar packing. Structural comparisons of β-CuPc, HP-CuPc, and η-CuPc are shown in fig. S3, C to H. This structural configuration with a smaller slip angle and more effective π stacking is highly favorable for topochemical polymerization along the stacking direction (*29*, *30*).

At 21.5 GPa, the lattice parameter *b* was compressed by 35.5% relative to that of the β-CuPc under ambient conditions, reaching 3.09 Å, whereas *a* and *c* underwent minimal changes (fig. S2C). Notably, this compression was quantitatively matched by the macroscopic geometric change of the single crystal (Fig. 2, C and D), and this anisotropic compression is consistent with the typical compression behavior observed along the polymerization direction of DNThs (*31*, *32*). Above 21.5 GPa, the crystal shrinks rapidly along the *b* axis, accompanied by a sharp deterioration of single-crystal diffraction signals, both indicating the onset of polymerization. Instead of further compression, we adopted thermal activation to achieve complete conversion, which prevents crystal fragmentation induced by the shrinkage of the sample chamber. After being heated to 533 K under 25.0 GPa, the crystal undergoes an irreversible contraction of ~46% along its elongation direction, corresponding to a reduction in the *b*-axis length to 2.57 Å. This length was largely retained when the sample was recovered to

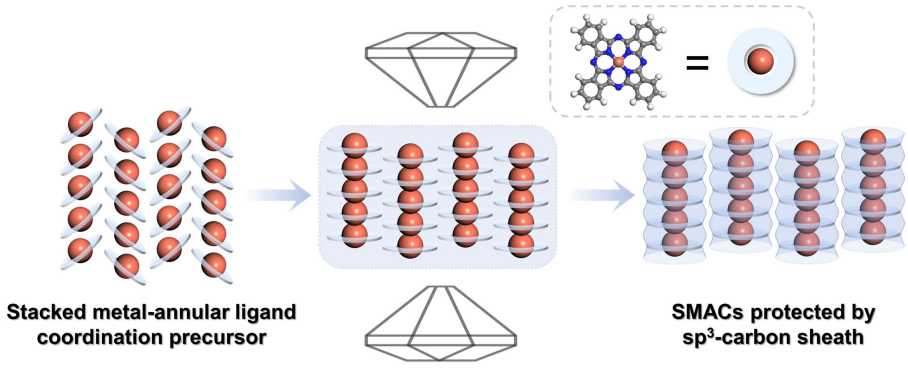

Fig. 1. Schematic illustration of the construction of a sSMAC from metal-annular ligand coordination precursors. High-pressure polymerization of organic molecules "locks in" the densely packed metal-chain structure, which persists even after pressure release.

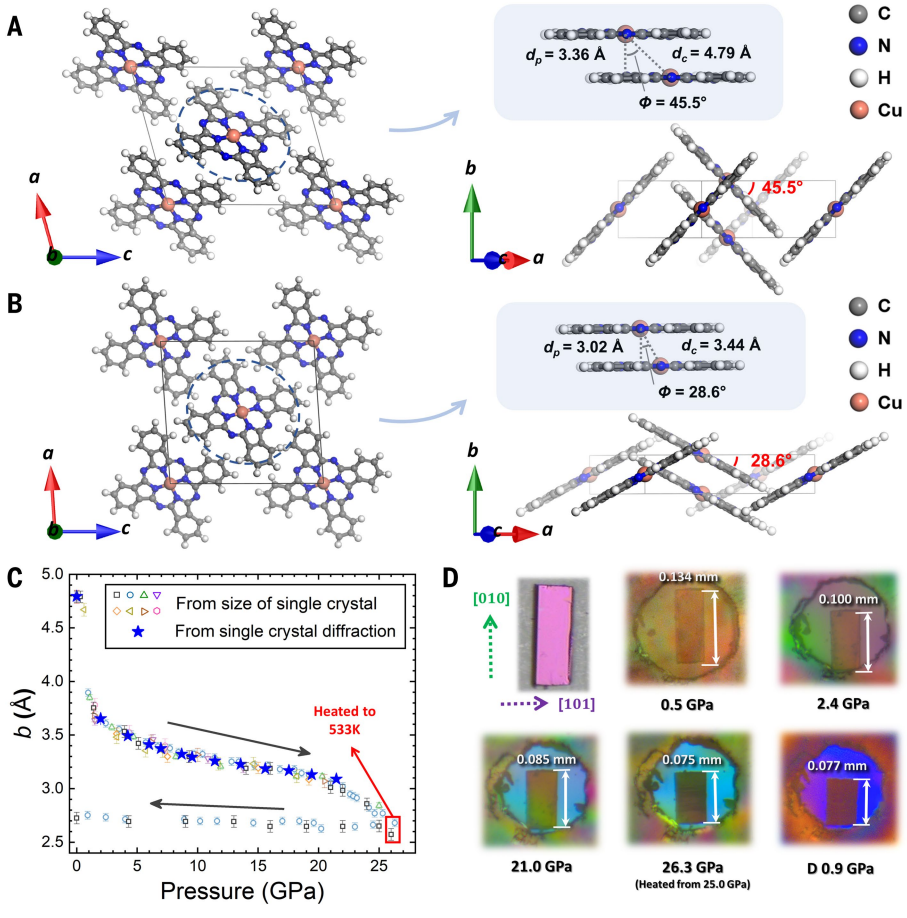

Fig. 2. Phase transition and polymerization of CuPc under high pressure. (**A** and **B**) Crystal structures of CuPc at ambient pressure (A) and 4.3 GPa (B). The relative orientation between adjacent CuPc molecules is described by the centroid distance (d_c; also the Cu-Cu distance), the interplanar distance (d_p), and the slip angle (Φ) between the molecular plane normal and the centroid vector. (**C**) Evolution of the lattice parameter *b* for single-crystal β-CuPc, determined by SCXRD and crystal dimension analysis. The data point marked in red were collected after heating to 533 K at 25.0 GPa, which induced a slight pressure increase. Different labels correspond to different experimental trials. (**D**) Optical images of a β-CuPc crystal during in situ compression-decompression.

ambient pressure. This is a typical periodicity of carbon nanothreads (*33*, *34*), just corresponding to that of two C-C bonds with an angle of 109°, and it strongly supports that β-CuPc polymerizes along the elongation direction and forms 1D nanowires with an apparent critical pressure around 21.5 GPa.

In situ infrared spectroscopy confirmed the polymerization by revealing sudden broadening of the absorption peaks of β-CuPc above 21 GPa (fig. S4A). After heating to 533 K at 25.0 GPa for 12 hours, the precursor's infrared signals disappear completely, thus confirming the completion of the reaction. The sample recovered to ambient pressure (DAC-25H) displays a strong infrared absorption peak near 2897 cm^{-1}, corresponding to sp^3 C-H stretching vibrations. By contrast, the sp^2 C-H stretching vibration near 3050 cm^{-1} is virtually absent (fig. S4B). These findings demonstrate that all the unsaturated C(-H) atoms on the periphery of the phthalocyanine rings polymerized, like many aromatics under external pressure (*24*, *25*), forming a saturated carbon sheath.

Structural characterization of Cu-sSMACs

The in situ characterizations of CuPc described in the previous section were mainly based on diamond anvil cells (DACs), which are good for optical observation but cannot support the scalable synthesis of sSMACs. To scalably synthesize large crystals, we compressed the β-CuPc single crystals to 40 GPa using a Paris-Edinburgh (PE) press, which yields milligram-scale large-size single-crystal Cu-sSMACs (PE-40, with maximum dimensions of ~940 μm by 250 μm by 50 μm; Fig. 3A). The infrared spectrum of the resulting product closely resembles that of DAC-25H, confirming structural consistency (fig. S4B). The obtained bulk PE-40 single crystal was characterized by laboratory SCXRD, revealing a 2D lattice formed by the aligned nanowires with unit cell parameters $a = 18.44$ Å, $c = 18.51$ Å, and $\beta = 91.24°$ (fig. S5). The periodic 1D array of Cu-sSMACs was also observed with an interchain *d* spacing of ~13.59 Å in the high-angle annular dark-field scanning transmission electron microscopy (HAADF-STEM) and selected-area electron diffraction (SAED) experiment, which corresponds to the $(10\bar{1})$ plane (Fig. 3, B and C). These results demonstrate the high structural ordering of the Cu-sSMACs formed through single crystal–to–single crystal polymerization of β-CuPc.

The SCXRD of PE-40 also revealed a periodicity of 2.57 Å along the nanowire axis, consistent with the $d = 2.50$ Å diffraction resolved from SAED patterns acquired perpendicular to the nanowire axis (Fig. 3C and fig. S5). This periodicity of 2.57 Å corresponds to the very close Cu-Cu distance, indicating that the carbon sheath preserves the highly compressed 1D metal chain formed under high-pressure conditions. The Cu-Cu distance constrained by the polymeric framework is substantially smaller than that of CuPc at

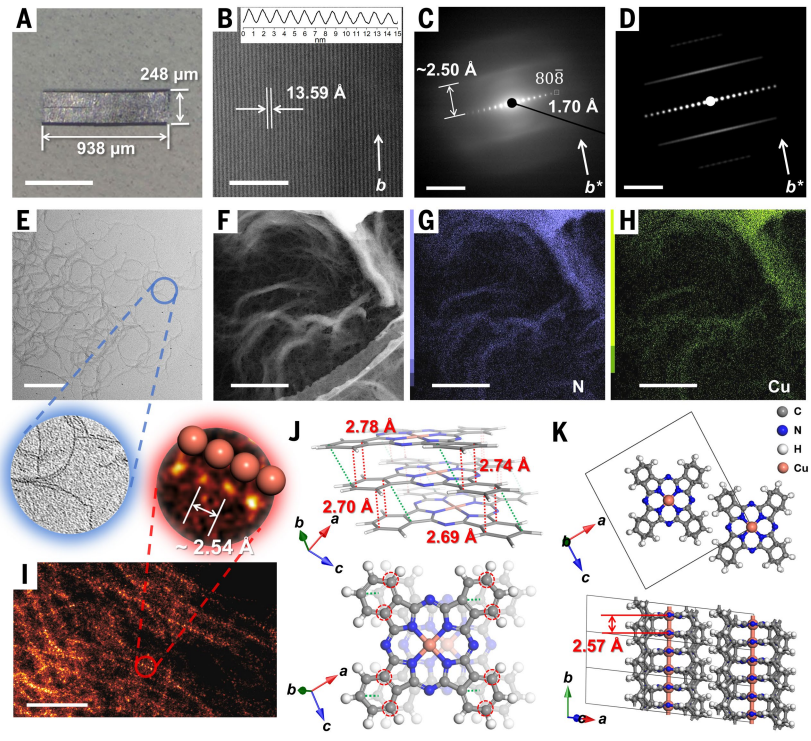

Fig. 3. Synthesis and structural characterization of large-scale Cu-sSMAC single crystals. (**A**) Optical images of a large-scale Cu-sSMAC single crystal (PE-40) synthesized from β-CuPc. Scale bar, 500 μm. (**B**) HAADF-STEM image of PE-40. Scale bar, 20 nm. (**C**) Experimental SAED pattern of PE-40 approximately along the [101] zone axis. Scale bar, 5 nm^{-1}. (**D**) Simulated SAED pattern of Cu-sSMACs incorporating interchain misalignment. Scale bar, 5 nm^{-1}. (**E**) HRTEM image of the PE-40 treated with TFA. The local magnification image below shows the structure of individual nanowires. Scale bar, 100 nm. (**F** to **H**) HAADF-STEM image (F) and corresponding EDS elemental maps [(G) and (H)] of PE-40 after TFA-assisted ultrasonication. Scale bars, 200 nm. (**I**) HAADF-STEM image of exfoliated wires from PE-40, where the chain-like arrangement of copper atoms within the nanowire is clearly visible. Scale bar, 5 nm. (**J**) Critical crystal structure of CuPc at 21.5 GPa. The shortest intermolecular C···C distances are highlighted by red dashed lines or circles. Possible bonding configurations are indicated by red and green dashed lines. (**K**) Polymer-I model of Cu-sSMACs with double nanowires contained in unit cells.

21.5 GPa, mimicking that of CuPc at 52 GPa by linearly extrapolating the lattice parameter *b* with pressure, as indicated in fig. S2D, which can be considered to be a "chemical pressure" of 52 GPa on Cu^{2+} to some extent. Notably, in both the SCXRD and SAED results, the diffraction patterns are sharp in the *h0l* plane but show a "layer line" structure on the *hkl* ($k \neq 0$) plane. This is attributed to the corelated disordering in the crystal—that is, every Cu-sSMAC exhibits an intrathread period of 2.57 Å along the *b* axis and is orderly stacked perpendicular to the *a-c* plane but undergoes partial disordered shifting along the *b* axis. This is a characteristic feature in 1D carbon nanothreads (*35*, *36*), and we can perfectly reproduce the diffraction pattern by simulation using such an orderly stack–disorderly shift model (Fig. 3D and fig. S6). Such a feature also suggests that the interthread interaction is relatively weak, which provides opportunity for exfoliation.

Typically, the low-dimensional nanomaterials synthesized through high-pressure methods are too dense for conventional exfoliation, especially for single crystal products. In this work, using a trifluoroacetic acid (TFA)–N-methyl-2-pyrrolidone (NMP) combined with ultrasonication, we effectively exfoliated the bulk single crystals (PE-40) and yielded individual nanowires. By protonating the bridging nitrogen atoms in their framework, TFA substantially increases the solubility of metal phthalocyanines in conventional solvents (*37*–*39*). Similarly, the exfoliation of Cu-sSMACs is likely driven by TFA-induced protonation of the analogous bridging nitrogen atoms in the phthalocyanine structure (fig. S7A) accompanied by lattice expansion. High-resolution transmission electron microscopy (HRTEM) images reveal plenty of narrow and curved 1D structures with widths around 1.3 nm, consistent with the theoretical diameter of the Cu-sSMACs, which confirms the successful exfoliation (Fig. 3E). The directly observed Cu-sSMAC detaching from the lattice has a length of >1 μm (fig. S7B), corresponding to more than 4000 Cu atoms, which surpasses the reported dimensions of SMACs by two to three orders of magnitude. This represents the first observation of isolated carbon nanowires synthesized under high pressure in a scalable manner since the initial account of DNThs in 2015 (*24*), a breakthrough that stands as a landmark in the development and application of high-pressure carbon nanomaterials. Notably, the Cu-sSMACs remain structurally intact after hours of ultrasonication in a highly acidic environment (2.7 M TFA in NMP; see materials and methods in the supplementary materials). Their exceptional stability, afforded by the saturated carbon scaffold, is further evidenced by energy-dispersive spectrometer (EDS) analysis (Fig. 3, F to H) and distinct Cu-sSMAC structure in HAADF-STEM (fig. S7, C and D). Under low-voltage and low-dose electron beam conditions, the Cu chain within individual wire was directly observed using HAADF-STEM. The measured Cu-Cu distance of 2.54 Å is in good agreement with other experimental results (Fig. 3I).

To figure out the structural model of the product, the crystal structure of CuPc at the critical pressure (21.5 GPa) was optimized by density functional theory (DFT) calculation with the lattice parameters fixed at the experimental result (a = 15.33 Å, b = 3.09 Å, c = 16.17 Å, and β = 93.4°, as determined by SCXRD). The intermolecular slip angle decreased to 27.1°, and the shortest C···C distance between adjacent CuPc molecules is measured to be 2.69 Å, which is substantially shorter than the typical critical distance (2.8 Å) required for aromatic molecular reactions (*40*) (Fig. 3J and fig. S8A).

On the basis of the closest interatomic distances between the adjacent Pc rings at this critical pressure, we proposed a structural model for the product, which was referred to as polymer-I by Chen *et al.* (*33*). In this model, the four benzene rings polymerize with those in the adjacent Pc rings, and the 18π-electron conjugated macrocycle is retained (fig. S8B). Structural optimization of this polymer-I model with released unit cell constraints produced a Cu-Cu distance of 2.57 Å and an ordered arrangement of Cu-sSMACs (Fig. 3K), both of which are in excellent agreement with experimental results, thereby confirming the model's reliability and structural fidelity (fig. S8C). Models with bonding between the 18π-electron conjugated macrocycle would substantially reduce the Cu-Cu distance, deviating from the TEM and crystallographic results. Furthermore, the infrared spectrum simulated from the polymer-I model is in excellent agreement with the experimental data. The absorption peak at 1533.5 cm^{-1}, assigned to the stretching vibration of the 18π-electron conjugated macrocycle (fig. S4C), is well preserved, demonstrating that the inner region of the Pc within the nanowire backbone remains in the sp^2-hybridized form.

To evaluate the bonding process, we performed a nudged elastic band calculation at 20 GPa and identified a transition state with an energy barrier of 50.3 kJ/(mol bonding), which is already lower than that of the typical room-temperature reaction (fig. S9A) (*41*). At 30 GPa, the barrier further decreases to 35.4 kJ/(mol bonding) (fig. S9B). Under these conditions, the π orbitals of the benzene ring substantially overlapped with those of adjacent benzene rings, forming σ bonds, and the whole CuPc column transforms into a Cu-sSMAC. This process is shown in movie S1. The simulation result is in good agreement with our experiments, which show that the polymerization initiated above

21 GPa. Notably, either elevated temperature or higher pressure applied during the synthesis of DAC-25H and PE-40 solely promote the completeness of the polymerization without altering the final reaction products. This conclusion is well verified by the highly consistent infrared, STEM, and SAED results obtained from the DAC-25H and PE-40 samples (Fig. 3, B to D; fig. S4B; and fig. S10).

Magnetism and electrical conductivity of Cu-sSMACs

To probe the Cu^{2+}-Cu^{2+} interactions, we measured the magnetic susceptibility of the PE-40. The sample exhibits an ~50% smaller magnetization compared with that of the precursor β-CuPc in the *M-H* curve (Fig. 4A). This reduction stems from the presence of antiferromagnetic interactions between closely spaced Cu^{2+} within the polymerized material. In the *M-T* curve, PE-40 shows a typical Curie-Weiss paramagnetism above 100 K, with a Weiss constant θ_{CW} of −34.2 K, signifying antiferromagnetic coupling (Fig. 4B) (*42*). By contrast, the *M-T* susceptibility data of β-CuPc also show a Curie-Weiss paramagnetism but a near-zero Curie-Weiss temperature ($\theta_{CW} \approx 0.008$ K) (fig. S11A), consistent with the literature (*43*).

Then we characterized the anisotropic electrical transport properties of the PE-40 single crystal along and perpendicular to the nanowire direction using ac impedance spectroscopy (Fig. 4C and fig. S11B) and fitted the data using the equivalent circuit shown in fig. S11C. The fitted capacitance values are consistent with the characteristics of grain boundary impedance in both directions (8.4×10^{-10} F/cm parallel to the *b* axis and 8.1×10^{-11} F/cm perpendicular to the *b* axis) (*44*), which indicates that the grain boundary or defect in the single crystal still dominates the resistance. The fitted resistance of grain boundary is $R_{gb,\parallel} = 9.0 \times 10^6$ ohms (5.5×10^{-3} S/m for conductivity) along the chain direction and $R_{gb,\perp} = 2.9 \times 10^7$ ohms (3.1×10^{-4} S/m) in the perpendicular direction, revealing a strong anisotropy of more than one order of magnitude. The intrinsic resistance of the grain R_g should be estimated from the high-frequency end (left end) of the semicircle; however, this value is approaching zero in the plot, which suggests a value that is orders of magnitude smaller. It should be noted that these are only preliminary observations. Obviously, samples with fewer grain boundaries or defects (smaller R_{gb}) are required for precise determination, and we need to use theoretical calculations to estimate the conductivity.

To understand the intrinsic magnetism and electronic properties of sSMACs, we performed spin-polarized DFT band structure calculations of the Cu-sSMACs and obtained the projected band structure and the projected density of states (PDOS), as shown in Fig. 4, D and E, and fig. S12A. The spin contribution is mainly from the $d_{x^2-y^2}$ orbital of Cu atoms and presents a prominent spin-alternating 1D chain in

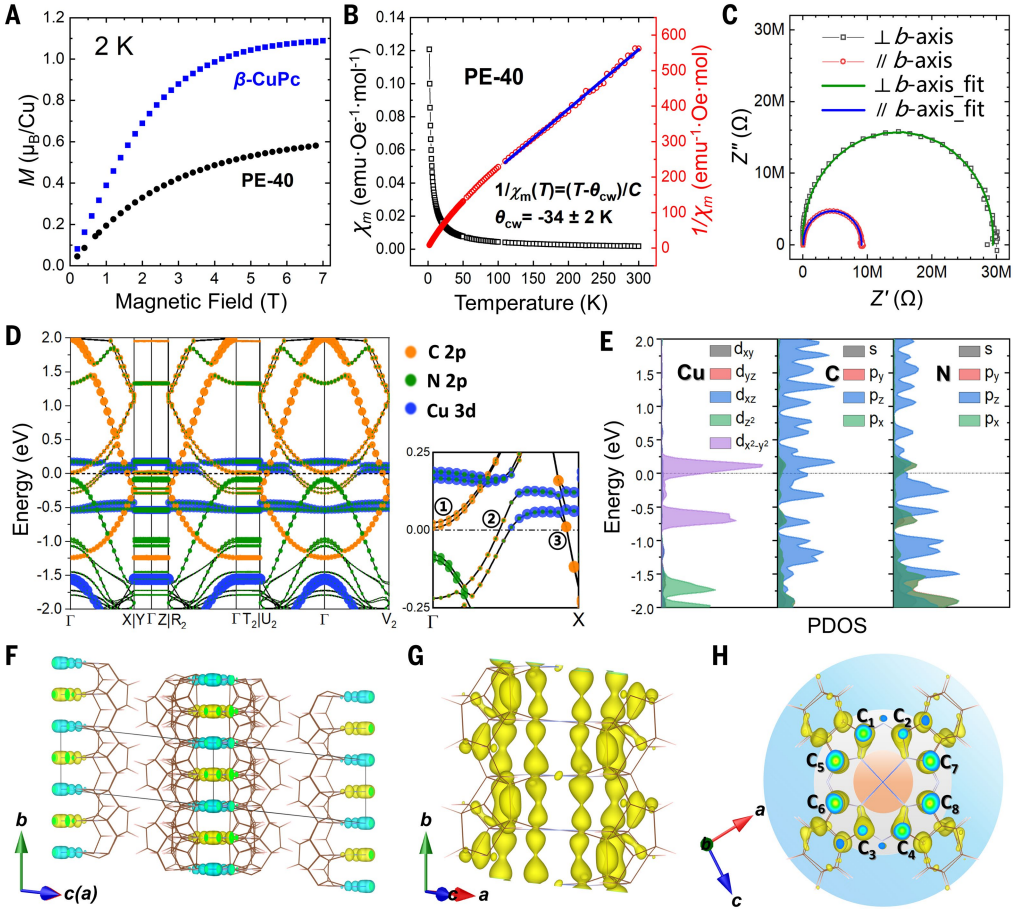

Fig. 4. Magnetic and electronic properties of Cu-sSMACs probed by experiments and computations. (**A**) Magnetic moment per Cu atom of PE-40 and β-CuPc as a function of field at 2 K. (**B**) Temperature-dependent magnetization of PE-40 fitted using the Curie-Weiss (CW) law. (**C**) Impedance spectra of PE-40 along *b* (||*b*) and perpendicular to *b* (⊥*b*) in Nyquist plots at room temperature. (**D**) Projected band structure of Cu-sSMACs, with the band weights from C 2p, N 2p, and Cu 3d orbitals. The inset magnifies the energy region from −0.25 eV to 0.25 eV along the Γ-X direction. Three groups of bands that provide the major contributions to electrical conduction are labeled as 1, 2, and 3. (**E**) PDOS for the orbitals of Cu, C, and N. (**F**) Spin density isosurfaces at ±0.007 e/Å^3. Yellow and cyan isosurfaces denote spin-up and spin-down densities, respectively. (**G**) Isosurface plot of the probability density for band 3 at the Γ point. The isosurface value is set to 0.0008 Å^{-3}, showing a pseudo−σ bonding chain formed by C 2p orbitals. (**H**) Schematic illustration of the triple-core-shell structure of Cu-sSMACs. The carbon atoms making predominant contributions to electrical conduction are labeled as C_1 through C_8 in the figure.

the spin density map at 0 K (Fig. 4F), which explains the substantial antiferromagnetic coupling between the Cu ions. To evaluate the Cu-Cu interaction, we performed a crystal orbital Hamilton population (COHP) analysis. The calculated integrated COPH (ICOHP) value is −0.27723 eV, suggesting that the bonding between the Cu atoms is very weak, consistent with the reported reluctance of Cu^{2+} to form metal-metal bonds (*19*). The e_g band of Cu is very flat (Fig. 4D) with a local electronic configuration and a gap of ~0.44 eV, which suggests that the conductivity of Cu-sSMACs does not rely on the metal-metal bonding of Cu.

By contrast, there are three bands (in orange) that cross the Fermi level and dominate the conductivity along the sSMACs. All of these bands have a parabolic shape, which is a typical feature of a nearly free electron model. In real space, these bands mainly come from C_1 to C_8 in Fig. 4H. These carbons are sp^2 hybridized and bonded to two N and one C atoms. The remaining 2p electron has a substantial interaction with the corresponding carbon atoms of the two neighbored units along the sSMACs, arguably forming a chain (Fig. 4G and fig. S12, B and C). Calculations of the electrical conductivity also show that the conductivity along the chain axis reached as high as 2.5×10^7 S/m, which is three orders of magnitude greater than that perpendicular to the nanowire direction (1.2×10^4 S/m). This represents the intrinsic upper bound for an ideal defect-free structure, highlighting the great potential of this system. Our experimental and computational results indicate that Cu-sSMACs have a distinct core structure sheathed by a saturated carbon framework, forming a three-layer architecture composed of an insulating shell, a conductive intermediate layer, and an antiferromagnetic core (Fig. 4H).

Conclusions

Using the unsaturated annular metal complex β-CuPc as a precursor, we synthesized extended Cu-sSMACs sheathed by a saturated carbon framework using a single-step compression. This pressure-induced polymerization process of CuPc is also applicable to other metal-Pc (MPc) complexes if the MPc molecules have a similar stacking. We compressed CoPc, NiPc, ZnPc, and H_2Pc that share similar structure with CuPc, and similar sSMACs were obtained (fig. S13). This indicates that the sSMAC is a 1D platform that can accommodate many kinds of metals. Mixed-metal–sSMAC and hetero-sSMAC junctions with multiple metal elements can also be expected. Our work proposes a universal strategy for the scalable synthesis of the ultralong, atom-scale, ordered, and ambient-stable SMACs, which can inspire a fresh perspective in exploring the fundamental physics and the distinctive properties of the 1D system and pave the way for potential applications in nanoelectronics devices.

REFERENCES AND NOTES

1. V. P. Georgiev, P. J. Mohan, D. DeBrincat, J. E. McGrady, *Coord. Chem. Rev.* **257**, 290–298 (2013).
2. R. Requist *et al.*, *Nat. Nanotechnol.* **11**, 499–508 (2016).
3. P. Gambardella *et al.*, *Nature* **416**, 301–304 (2002).
4. A. Cornia *et al.*, *Inorg. Chem.* **59**, 1763–1777 (2020).
5. A. Nicolini *et al.*, *Dalton Trans.* **50**, 7571–7589 (2021).
6. E. Cariati *et al.*, *Coord. Chem. Rev.* **306**, 566–614 (2016).
7. O. Hietsoi, A. S. Filatov, C. Dubceac, M. A. Petrukhina, *Coord. Chem. Rev.* **295**, 125–138 (2015).
8. C. Lin *et al.*, *Nat. Catal.* **4**, 1012–1023 (2021).
9. E. B. Kolomeisky, J. P. Straley, *Phys. Rev. B* **53**, 12553–12555 (1996).
10. C. Blumenstein *et al.*, *Phys. Rev. Lett.* **107**, 165702 (2011).
11. C. Blumenstein *et al.*, *Nat. Phys.* **7**, 776–780 (2011).
12. S. A. Hua, Y. C. Tsai, S. M. Peng, *J. Chin. Chem. Soc.* **61**, 9–26 (2013).
13. S. A. Hua, M. C. Cheng, C. Chen, S. M. Peng, *Eur. J. Inorg. Chem.* **2015**, 2510–2523 (2015).
14. M. Ma *et al.*, *Cell Rep. Phys. Sci.* **3**, 101124 (2022).
15. D. R. Belcher, M. W. Radny, S. R. Schofield, P. V. Smith, O. Warschkow, *J. Am. Chem. Soc.* **134**, 15312–15317 (2012).
16. S. Guo *et al.*, *Nat. Synth.* **1**, 245–253 (2022).
17. W. Qin *et al.*, *Nat. Commun.* **16**, 4924 (2025).
18. J. K. Bera, K. R. Dunbar, *Angew. Chem. Int. Ed.* **41**, 4453–4457 (2002).
19. M. Stollenz, *Chemistry* **25**, 4274–4298 (2019).
20. R. H. Ismayilov *et al.*, *Angew. Chem. Int. Ed.* **50**, 2045–2048 (2011).
21. K. Zeng *et al.*, *Angew. Chem. Int. Ed.* **62**, e202216060 (2023).
22. Y. Zhang, K. Zeng, Y. Wu, F. Huang, H. Peng, *Sci. Bull.* **70**, 2223–2227 (2025).
23. W. Zhao *et al.*, *CCS Chem.* **7**, 1250–1271 (2025).
24. T. C. Fitzgibbons *et al.*, *Nat. Mater.* **14**, 43–47 (2015).
25. D. Gao *et al.*, *Proc. Natl. Acad. Sci. U.S.A.* **119**, e2201165119 (2022).
26. X. Wang *et al.*, *J. Am. Chem. Soc.* **144**, 21837–21842 (2022).
27. H. Wang *et al.*, *ACS Nano* **4**, 3921–3926 (2010).
28. T. Zou *et al.*, *Crystals* **8**, 22 (2018).
29. W. S. Tang, T. A. Strobel, *J. Phys. Chem. C* **124**, 25062–25070 (2020).
30. X. Yang *et al.*, *Chem* **12**, 102836 (2026).
31. S. G. Dunning *et al.*, *Angew. Chem. Int. Ed.* **62**, e202217023 (2023).
32. A. Friedrich *et al.*, *J. Am. Chem. Soc.* **142**, 18907–18923 (2020).
33. B. Chen *et al.*, *J. Am. Chem. Soc.* **137**, 14373–14386 (2015).
34. B. Chen *et al.*, *J. Chem. Theory Comput.* **14**, 1131–1140 (2018).
35. M. D. Ward *et al.*, *Macromolecules* **52**, 7557–7563 (2019).
36. S. J. Juhl *et al.*, *J. Am. Chem. Soc.* **141**, 6937–6945 (2019).
37. H. Yamanouchi, K. Irie, T. Saji, *Chem. Lett.* **29**, 10–11 (2000).
38. K. P. Srivastava, A. Kumar, *Asian J. Chem.* **13**, 1539–1543 (2001).
39. N. K. Shrestha *et al.*, *Langmuir* **26**, 17024–17027 (2010).
40. X. Tang *et al.*, *Matter Radiat. Extremes* **8**, 058402 (2023).
41. M. Podewitz, *Nat. Synth.* **4**, 913–921 (2025).
42. S. Mugiraneza, A. M. Hallas, *Commun. Phys.* **5**, 95 (2022).
43. S. Heutz *et al.*, *Adv. Mater.* **19**, 3618–3622 (2007).
44. J. T. S. Irvine, D. C. Sinclair, A. R. West, *Adv. Mater.* **2**, 132–138 (1990).

ACKNOWLEDGMENTS

Funding: The authors acknowledge the support of the National Key Research and Development Program of China (no. 2023YFA1406200) and the National Natural Science Foundation of China (NSFC) (no. 22022101). X.D. and S.Q. acknowledge support from the NSFC (no. 12574019) and the Academy for Advanced Interdisciplinary Studies, Nankai University (nos. 9261500174 and 9261500166). S.J., Y.D., and Y.X. acknowledge support from the NSFC (nos. 22488101 and 22325503), Fundamental Research Funds for the Central Universities (no. 2024ZYGXZR004), and the Guangdong Provincial Quantum Science Strategic Initiative (no. GDZX2301002). The authors acknowledge the support of the Synergetic Extreme Condition User Facility (SECUF). This work was carried out with the support of the BL17UM beamline and BL14W1 beamline at the Shanghai Synchrotron Radiation Facility (SSRF) as well as the BL10XU beamline at Spring-8. The calculations were performed and supported by Tianhe II in Guangzhou. **Author contributions:** Conceptualization: K.L.; Formal analysis: J.Z., H.Z., K.L., S.Q., X.D., Q.Z., P.L., Y.W.; Funding acquisition: H.Z., K.L., H.-k.M.; Investigation: J.Z., X.D., S.Q., X.Y., C.L., H.M., Y.Fe., F.L., H.L., Q.Z., X.J., J.X., Y.B., Y.D., Y.X., Y.Fa., Z.Z.; Methodology: J.Z., S.Q., X.Y., X.D., K.L.; Resources: J.Z., J.Y.; Supervision: K.L.; Visualization: J.Z., S.Q.; Writing – original draft: J.Z., H.Z., K.L.; Writing – review & editing: J.Z., H.Z., K.L., X.D., Y.C., S.J., J.S. **Competing interests:** The authors declare that they have no competing interests. **Data, code, and materials availability:** All data are available in the main text or the supplementary materials.

SUPPLEMENTARY MATERIALS

science.org/doi/10.1126/science.aeg0028
Materials and Methods; Figs. S1 to S13; Table S1; References (*45*–*64*); Movie S1

Submitted 2 February 2026; accepted 24 June 2026

10.1126/science.aeg0028

Ultralong sheathed single-metal-atom chains synthesized under high pressure

Jie Zhang, Xiao Dong, Shengchao Qiu, Xin Yang, Chengyu Li, Hongfei Ma, Yunfan Fei, Qingchao Zeng, Fang Li, Yi Xie, Yan Duan, Xudong Jiang, Jingqin Xu, Puyi Lang, Jiarui Yuan, Hao Luo, Yuan Fang, Zilin Zhao, Yikun Bao, Yajie Wang, Yongjin Chen, Junliang Sun, Shangda Jiang, Ho-kwang Mao, Haiyan Zheng, and Kuo Li

Science **393** (6813), . DOI: 10.1126/science.aeg0028

Editor's summary

Single-metal atom chains represent an attractive platform for building nanoscale electronics, but their practical use has been limited by synthetic challenges. Zhang *et al*. developed a high-pressure route that converts #-copper phthalocyanine into micrometer-long copper atomic chains encased in a carbon sheath. They showed that compression above 21 gigapascals polymerizes the organic framework and locks copper atoms into chains. The resulting nanowires exhibited strong anisotropic conduction and one-dimensional antiferromagnetic coupling. —Jack Huang